SAND2011-8294C

AIAA-99-0033

LOAD MITIGATION WITH TWIST-COUPLED HAWT BLADES

Don W. Lobitz
Principle Member of the Technical Staff
505-844-9398/dwlobit@sandia.gov
Sandia National Laboratories
Albuquerque, New Mexico 87185-0439

David J. Laino
Research Assistant Professor
801-585-7405/dlaino@stress.mech.utah.edu
University of Utah Department of Mechanical Engineering
Salt Lake City, Utah 84112

Abstract

The load mitigation prospects of a blade that twists toward feather as it bends is addressed in this paper. For this investigation, the ADAMS-WT software has been modified to include blade models with bending-twist coupling. Models of a representative rotor operating at a constant speed are developed for several values of the bending-twist coupling coefficient, all in a range that assures positive definiteness of the structural stiffness. Using the twist-coupled models, the ADAMS software is exercised for a spectrum of stochastic wind time series. This spectrum contains time series with three mean wind speeds at two turbulence levels. Fatigue damage calculations are done for the generated load histories using a range of material exponents that represent materials from welded steel to aluminum to composites, and results are compared with the damage computed for the rotor without twist-coupling. Power output for the various cases is also monitored to determine power deviations resulting from the coupling. Results indicate that for high but physically attainable levels of the coupling coefficient, significant reductions in damage are achieved across the spectrum of applied wind loading.

Introduction

In the process of improving HAWT performance, new methods are continually being sought for capturing additional amounts of energy, alleviating loads and controlling the rotor. One such technique employs the use of an adaptive blade that can sense the wind velocity or rotational speed in some fashion and accordingly modify its aerodynamic configuration to meet a desired objective. This could be achieved in either an active or passive manner, although the passive approach is much more attractive due to its simplicity and economy. As an example, a blade design might employ coupling between bending and/or extension, and twisting so that, as it bends and extends due to the action of the aerodynamic and inertial loads, it also twists modifying the aerodynamic performance in some way. Previous work has investigated increased energy capture for a constant speed rotor having twist-coupled blades. Lobitz and Veers[1] investigated the aeroelastic stability of these blades. Results of that study which focused on the Combined Experiment Blade (CEB) indicated that although the coupling generally had a destabilizing effect, the operating speed of that rotor was always below the speed at the stability boundary over a wide range of coupling levels.

Bolstered by these results, the current investigation addresses the load mitigation prospects of a blade that twists toward feather as it bends. Of course stall regulation will be more difficult if not impossible with this blade and therefor some other means of regulation is recommended. One possibility is variable speed operation which is becoming increasingly more popular with wind turbine designers.

As with the previous work, the analysis for the bending-twist coupled blade is carried out within the confines of beam finite element theory. The coupling terms for the beam elements are generated starting with beam "stress-strain" relations. For the bending-twist coupling the "stress-strain" relations at a point along the blade span are given by:

This work was supported by the United States Department of Energy, Sandia National Laboratories under Contract DE-AC04-94AL8500

$$\begin{bmatrix} EI & -g \\ -g & GK \end{bmatrix} \begin{bmatrix} \frac{\partial q}{\partial x} \\ \frac{\partial j}{\partial x} \end{bmatrix} = \begin{bmatrix} M_b \\ M_t \end{bmatrix} \quad (1)$$

Here, $q = \partial v / \partial x$ is the flapwise slope of the blade (v is the flapwise displacement), M_b is the flapwise bending moment, j is the blade twist, and M_t is the twisting moment. The material parameters *E* and *G* are the Young's modulus and the shear modulus respectively; *I* represents the moment of inertia of the cross section and *K* the torsional moment of inertia (equal to the polar moment of inertia for circular sections). The quantity, *g*, is the coupling term, and has a value of zero for the standard beam where no coupling is present. In order for this system to be positive definite (*i.e.*, the determinant of the matrix of Equation 1 must be greater than zero) *g* is taken to be:

$$g = a\sqrt{EIGK}, \quad -1 < a < 1 \quad (2)$$

The coupling coefficient, a, provides for variable coupling within the designated limits. Only bending in the flapwise direction is accounted for in Equation 1. Bending in the edgewise direction is considered to be small relative to the flapwise direction, yielding minimal coupling. Axial extension is also ignored for this type of coupling.

In order to use the ADAMS-WT software[2] to create rotor models for subsequent analysis with ADAMS[3] coupled with Aerodyn[4], modifications to incorporate the coupling in the "tapered beam" stiffness matrix are required. These modifications involve replacing the k_{46} and k_{64} elements of the matrix, which are normally zeroed, with the expression given below:

$$\frac{-(a_L + a_0)[(EI_L + EI_0)(GK_L + GK_0)]^{1/2}}{4L} \quad (3)$$

The subscripts *L* and 0 refer to the quantities evaluated at either end of the element. Further explanation of the other parameters in this expression can be found in Reference 2. The parameter α is also added to the "Rotor Blade Data File" to facilitate model input and provide for a coupling coefficient that varies with blade span. The above expression provides a mean value for the coupling in each blade element. As the mean value is only exact for the case of a uniform blade, the positive definiteness of the stiffness matrix may not be preserved for non-uniform blades with high absolute values of the coupling coefficient ($|\alpha| > 0.9$).

To verify that the coupling is incorporated in ADAMS-WT correctly, results for the CEB reported in Reference 1 have been reproduced with ADAMS. These results are associated with the CEB turning in still air over a range of bending-twist coupling levels. Blade tip rotations and deflections are shown in Figure 1 as a function of α for both the previously generated NASTRAN results and the current ADAMS results. The favorable agreement between the two provides confidence that the ADAMS modeling is correct.

Using a twist-coupled model of a representative stall-regulated rotor operating at a constant speed, ADAMS is exercised using stochastic wind time series generated with SNLWIND-3D[5] for hub-height mean wind speeds of 8 m/s, 14 m/s and 20 m/s. These wind speeds represent the linear aerodynamic, stall and post stall regions of the power curve, respectively. Two turbulence levels are used in the simulations, one representing the current IEC standard[6] and the other at 50% of that standard. These levels represent a relatively turbulent site and a relatively benign one. With these wind loadings, computations are completed for several values of the bending-twist coupling coefficient within a range that assures positive definiteness of the structural stiffness. These are α = -0.6, -0.3, 0.0, 0.3, 0.6, with α = 0.0 corresponding to the uncoupled case. Load histories and power output are computed and stored for all of the above cases for subsequent post processing.

Fatigue damage estimates are computed for these load histories assuming that damage is proportional to the load cycle amplitude raised to a material exponent, *b*. The parameter *b* is often used to define the fatigue behavior of a material that follows the trend:

$$N \propto S^{-b} \quad (4)$$

where *S* is the stress amplitude and *N* is the number of cycles to failure.

Values for *b* of 3, 6, and 9 are used to represent a range of materials from welded steel to aluminum to composites. The damage is assumed to be cumulative and therefor Miner's Rule is invoked. Damage results for the various levels of bending-twist coupling are compared to the uncoupled case. Average power levels and maximum load levels are also compared.

The remaining sections of the paper contain a description of the rotor model and wind inputs, computed results, and concluding remarks.

Table 1 - Model Configuration Summary

Parameter	Value
Number of blades	3
Rotor configuration	upwind
Yaw configuration	fixed
Blade length	14.9 m
Rotor hub radius	1.5 m
Rotor precone angle	0.0 deg
Rotor radius	16.4 m
Rotor hub height	50 m
Rotor tilt angle	0.0 deg
Rotor (constant) rotational speed	32 RPM

Rotor and Turbulence Models

The rotor model created using ADAMS WT employs fully flexible blades comprised of 20 elements each. All other model parts and interconnections are rigid. Parameters for the basic model are presented in Table 1. The rotor blade is based on an existing 15m-blade design, modified only to include the twist-coupling. No attempt was made to optimize this blade.

Models were created in ADAMS WT for each of the five twist-coupling, α, values discussed earlier. The pitch angle of the majority of these models is a constant 0.0 degrees. Power curves for three of these models are shown in Figure 2. Because α affects blade twist and therefor stall, it also affects the power curve for the model, as shown in Figure 2. An additional model was created for $\alpha = 0.6$ with a blade pitch of -4 degrees, to limit the peak power, and hence drivetrain loading, to that of the $\alpha = 0.0$ model. The power curve for this model is also shown in Figure 2.

An interesting feature of the $\alpha = -0.6$ power curve in Figure 2 is the instability near peak power (12 – 18 m/s), which apparently results from the onset of stall flutter. The effect of this instability on fatigue life will be discussed in the Results section.

Simulated turbulence was created using SNLWIND-3D for 3 average wind speeds as discussed earlier. Inputs to the program were chosen to duplicate conditions specified in the IEC standard. Shear velocity input was used to vary turbulence intensity. Ten 10-minute wind data sets were created at each wind speed for IEC turbulence intensity level, each using a different seed or initiation point for the random process utilized in generating the time series. Ten additional 10-minute turbulence files were created at each wind speed with the turbulence intensity set to 50% of IEC levels. Figure 3 compares the turbulence intensities of the simulated turbulence with the IEC criteria.

Table 2 - Non-Rotating Blade 1st Flap Frequencies

a	-0.6	-0.3	0.0	0.3	0.6
Freq.(Hz)	1.69	2.25	2.39	2.22	1.65

In all, a total of 100 minutes of simulated turbulence at each mean wind speed and turbulence level were created. Thus, with the six models investigated, a total of 3600 simulated minutes – comprised of 360 10-minute simulations – are used in this analysis.

Results

Simulation results discussed in this section include fatigue damage, average power and maximum load for the various cases. In addition to the damage estimates sample load spectra are provided. A sample load time history is also included that shows the development of a possible stall flutter instability.

Figures 4 (a, b, and c) and 5 (a, b, and c) summarize the fatigue damage for most of the simulations, Figure 4 for the high turbulence intensity corresponding to the IEC Standard and Figure 5 for half of that turbulence level. The damage is computed for the out-of-plane root bending moment only as the loads are generally highest at that location. Loads due to blade twist are not considered in the damage computation. For each turbulence intensity the damage is normalized to the damage that occurs for the 14 m/s wind speed and $\alpha = 0.0$. Thus in Figures 4b and 5b the damage associated with the $\alpha = 0.0$ bar is set to unity for all three values of the material exponent. In all cases positive α indicates twisting toward feather, and negative α, toward stall.

It is immediately apparent from Figures 4b and 5b that twisting to stall dramatically increases fatigue damage for the 14 m/s wind speed. This is probably the result of an apparent stall flutter instability that occurs for negative α in the stall and post stall wind regimes. As mentioned earlier, the power curve for $\alpha = -0.6$ in Figure 2 shows a region of instability from approximately 12 m/s out to 18 m/s. This instability is also apparent in the time series plot of Figure 6 for the out-of-plane moment. Here the frequency of the instability is approximately 1.7 Hz which is close to the frequency of the first bending-twist coupled mode of the $\alpha = -0.6$ blade, as listed in Table 2. For the 8 m/s and 20 m/s wind speeds, coupling toward stall still carries a high damage penalty although not as dramatic as that for

the 14 m/s wind speed, where stall events occur more often.

Comparing damage results for $\alpha = 0.0$ and $\alpha = 0.6$ (twisting toward feather), there is at least a factor of two reduction in damage in almost all cases with significantly greater reductions for the 8 m/s wind speed. For the case of $\alpha = 0.3$ the reductions in damage are proportionately much less than for those of $\alpha = 0.6$, especially for the 20 m/s wind speed. In general, the trend of reduced relative damage with increasing α is roughly independent of the material exponent.

Figure 5 a and b show the curious result that the relative damage for $b = 6$ and 9 is greater for some α's at 8 m/s than at 14 m/s. This is due to differences in the range of lift coefficient realized at different wind speeds and turbulence levels, as shown in Figure 7. For low turbulence, Figure 7(a) shows that at 8 m/s the blade operates in the linear part of the lift curve, covering a range from 0.6 to 1.4. At 14 m/s the blade operates in stall transition covering the smaller range from 1.2 to 1.6. Therefore, although the loads are in general greater at 14 m/s, loads cycles are actually larger at 8 m/s. Figure 7(b) shows that the lift curve range for 14 m/s is much greater for the higher turbulence level – 0.6 to 1.6 – than for the lower turbulence level, hence this result of higher damage at lower wind speed is not evident in Figure 4.

Figure 8 shows load spectra for $\alpha = -0.6, 0.0, 0.6$ for the 14 m/s average wind speed with IEC turbulence intensity. Cycle amplitude clearly increases with decreasing α, and the effect of the instability for $\alpha = -0.6$ discussed above is dramatic.

Figure 9 provides comparisons of the maximum bending moments that occur in each time series for the various α's and average wind speeds. For each wind speed the maximum load for $\alpha = 0.6$ is somewhat less than that for $\alpha = 0.0$. The random nature of the turbulence can make such a direct comparison of maximum values misleading. A better way to compare the maxima is using probability of exceedence curves. These were calculated using a Gumbel distribution fit from the FITS routine[7] and are shown in Figure 10 for the 20 m/s case. It is clear that the probability of exceeding a given maximum load value tends to decrease with increasing alpha.

In Figure 11 the average power is displayed for the various cases and, except for the average wind speed of 8 m/s, the average power is greater for $\alpha = 0.6$ than for $\alpha = 0$. This result is consistent with the power curves of Figure 2.

In short summary, for a blade that twists to feather as it bends with a bending-twist coupling coefficient of $\alpha = 0.6$, the rotor produces greater average power and simultaneously experiences smaller maximum loads and half the fatigue damage when compared to the uncoupled blade. While these are all very desirable improvements, a higher capacity gearbox and generator would be required to accommodate the higher power of this twist-coupled rotor. Additionally, as observed from its power curve in Figure 2, this rotor does not stall regulate and therefor some other means of regulation would be necessary.

To obtain a more rigorous comparison, the blade pitch of the above twist-coupled rotor was adjusted toward stall to obtain a power curve similar to the one for the uncoupled rotor. This is accomplished by setting the pitch of the twist-coupled rotor to -4.0 degrees. The resulting power curve, shown in Figure 2, is now in reasonable agreement with the one for the uncoupled rotor. As shown in Figure 9, the maximum loads for the pitched blade rotor with $\alpha = 0.6$ have crept up a little higher than those of the unpitched, $\alpha = 0.6$ model, and are now roughly equivalent to those for the uncoupled rotor. The probability of exceedence for a given maximum load also increases slightly for the pitched blade as shown in Figure 10. Likewise, as shown in Figure 11, the average power levels have crept down some and are also roughly equivalent to those for the uncoupled rotor (this is expected since the two power curves are now roughly equivalent). However, referring to Figures 4 and 5 (a, b, and c), the fatigue damage levels for nearly all cases shown are still down by at least a factor of two when compared to those of the uncoupled rotor. Thus in this case the primary improvement provided by the twist-coupled blade is a substantial reduction in fatigue damage.

Conclusions and Recommendations

The ADAMS software is employed to investigate the feasibility of using blades that twist as they bend to mitigate fluctuating loads. Time series calculations are made for three average hub-height wind speeds, two wind turbulence settings and five levels of twist-coupling. Fatigue damage is computed from the load histories using material exponents that represent materials ranging from welded steel to composites.

Results show that twist-coupling toward stall produces significant increases in fatigue damage, and for a range of wind speeds in the stall regime apparent stall flutter behavior is observed. For twist-coupling toward feather with a coupling coefficient of 0.6 fatigue damage is decreased by at least a factor of two for almost all of the cases investigated. The damage reductions seemed to be relatively independent of the material exponent.

Concurrent with lower fatigue damage estimates for positive twist-coupling, maximum loads decreased modestly and average power increased due to elevations in the power curve in the stall region. When the pitch is altered to bring the power curve into agreement with that of the uncoupled rotor, fatigue damage levels remain at the same reduced levels while differences in maximum load and average power are reduced.

There is evidence in the power curve that pitching the coupled rotor may reduce overall energy capture. However, for a new rotor, twist-coupled blades would be carefully designed to minimize this reduction. Also, the use of twist-coupling along with active turbine power control could better take advantage of the increased energy capture seen in these results, while maintaining the fatigue load mitigation observed.

The turbine model used was a simple one, making it difficult to extrapolate results to machines incorporating variable speed, pitch control, or non-zero rotor coning. The substantial fatigue damage reductions that have been predicted call for additional investigation, and turbines incorporating these increasingly common characteristics should be included. The combination of rotor coning and variable speed is especially interesting, as twist will vary with rotor speed due to flap loading caused by centrifugal force.

The fatigue benefits of twist-coupling can only be realized if blades incorporating this trait can be built. Composite, uniform, D-spars have already been designed and fabricated[8] that possess coupling coefficients in the range of 0.6. The next step involves the design and fabrication of a much more complex twist-coupled blade with a coupling coefficient in this same range. Design factors such as span-wise variance of coupling coefficient, and optimization of blade geometry to make the most of the advantages of twist-coupling need to be investigated. The ultimate goal is to design and produce a rotor blade that provides maximum benefit to turbine performance with minimal additional production cost.

References

1. D. W. Lobitz, and P. S. Veers, "Aeroelastic Behavior of Twist-Coupled HAWT Blades," Proceedings of the 1998 ASME Wind Energy Symposium, Reno, January 12-15, 1998.

2. ADAMS/WT User's Guide, Version 1.50, Mechanical Dynamics, Inc., Ann Arbor, February 1997.

3. ADAMS/SOLVER Reference Manual, Version 8.0, Mechanical Dynamics, Inc., Ann Arbor, November 15, 1994.

4. A. C. Hansen, AeroDyn for ADAMS User's Guide, Version 11.0, University of Utah, Salt Lake City, August 31, 1998.

5. N. D. Kelley, "Full-Vector (3-D) Inflow Simulation in Natural and Wind Farm Environments Using an Expanded Version of the SNLWIND (Veers) Turbulence Code," Proceedings of the 12th ASME Wind Energy Symposium, Houston, 1993.

6. Safety of Wind Turbine Generator Systems, International Electrotechnical Commission, IEC 61400-1, Second Edition, 1998.

7. T. Kashef and S.R. Winterstein, Moment Based Modeling and Extreme Response Estimation – The FITS Routine, Report No. RMS-31, Civil Engineering Dept., Stanford University, 1998.

8. C. H. Ong and S. W. Tsai, "Design, Manufacture and Testing of a Bend-Twist D-Spar," Proceedings of the 1999 ASME Wind Energy Symposium, Reno, January 11-14, 1999.

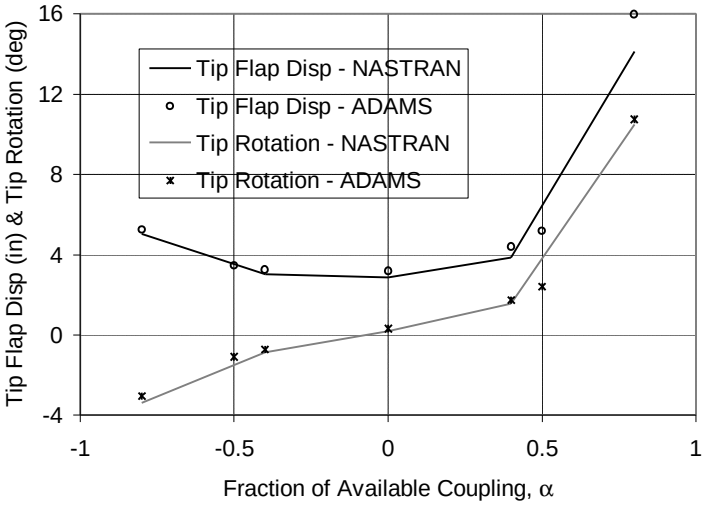

Figure 1. ADAMS/NASTRAN comparison for the CEB with bending-twist coupling.

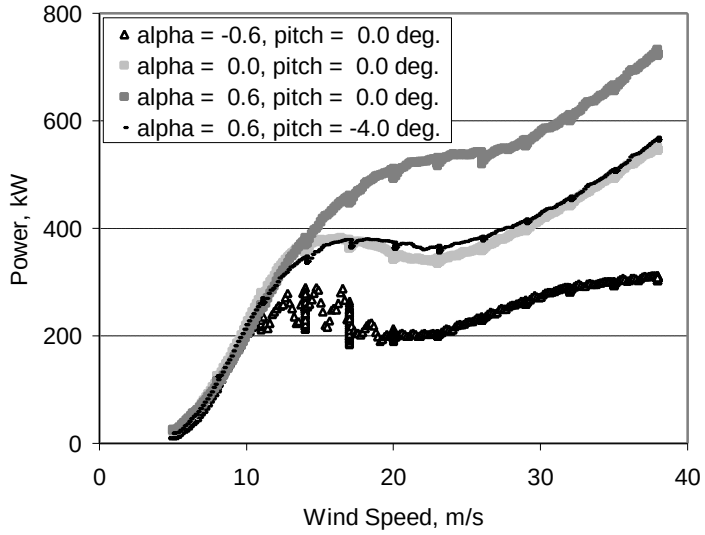

Figure 2. Power curves for 4 models demonstrating effect of twist-coupling (α) and pitch angle.

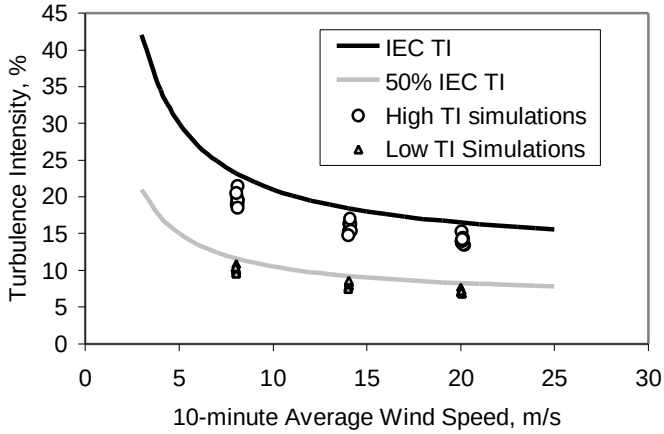

Figure 3. Turbulence intesity of simulated turbulence compared to IEC standard criteria.

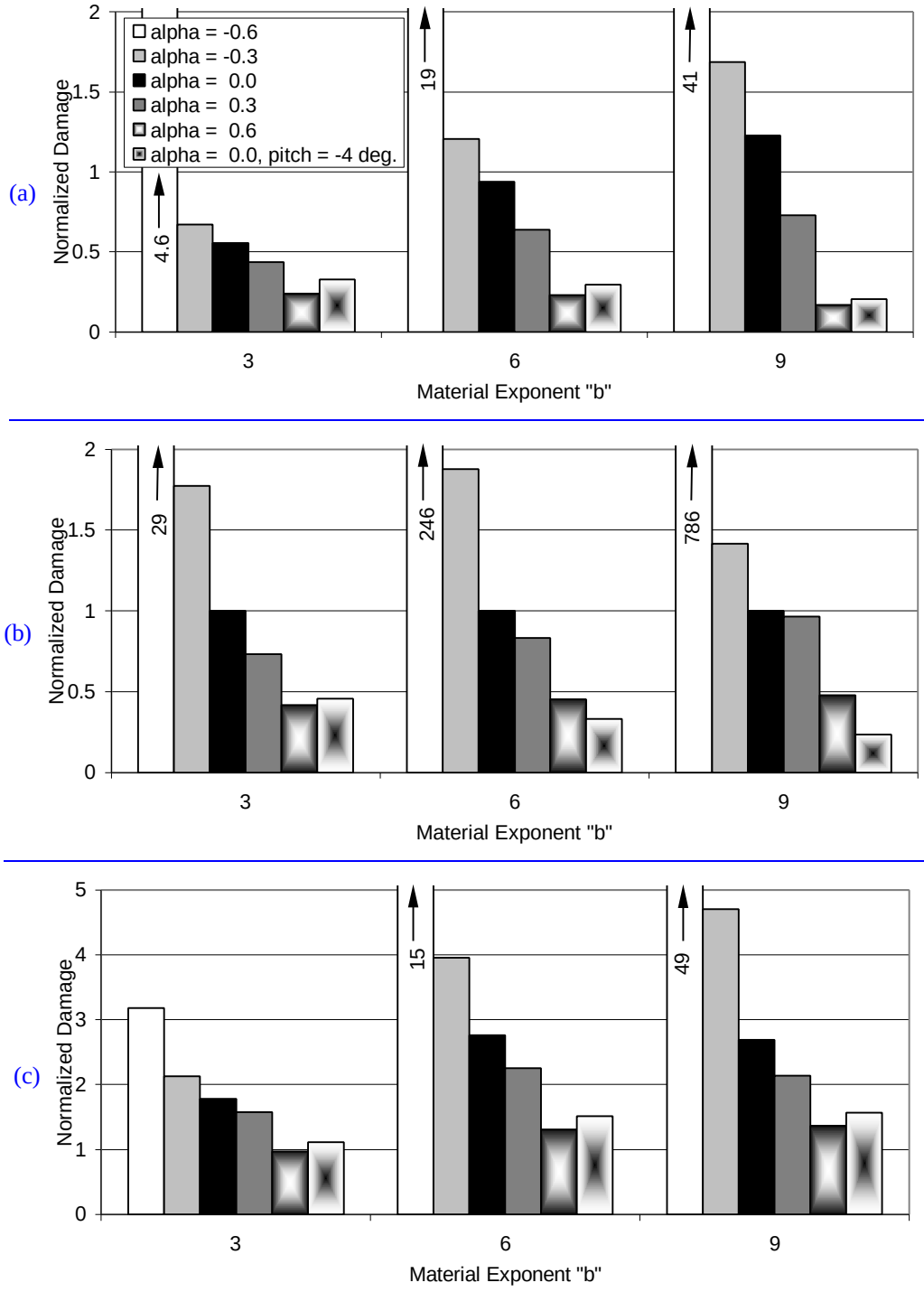

Figure 4. Comparison of relative fatigue damage for 6 blade models and 3 material exponents for 100 simulated minutes at (a) 8, (b) 14, and (c) 20 m/s average wind speed with IEC turbulence intensity.

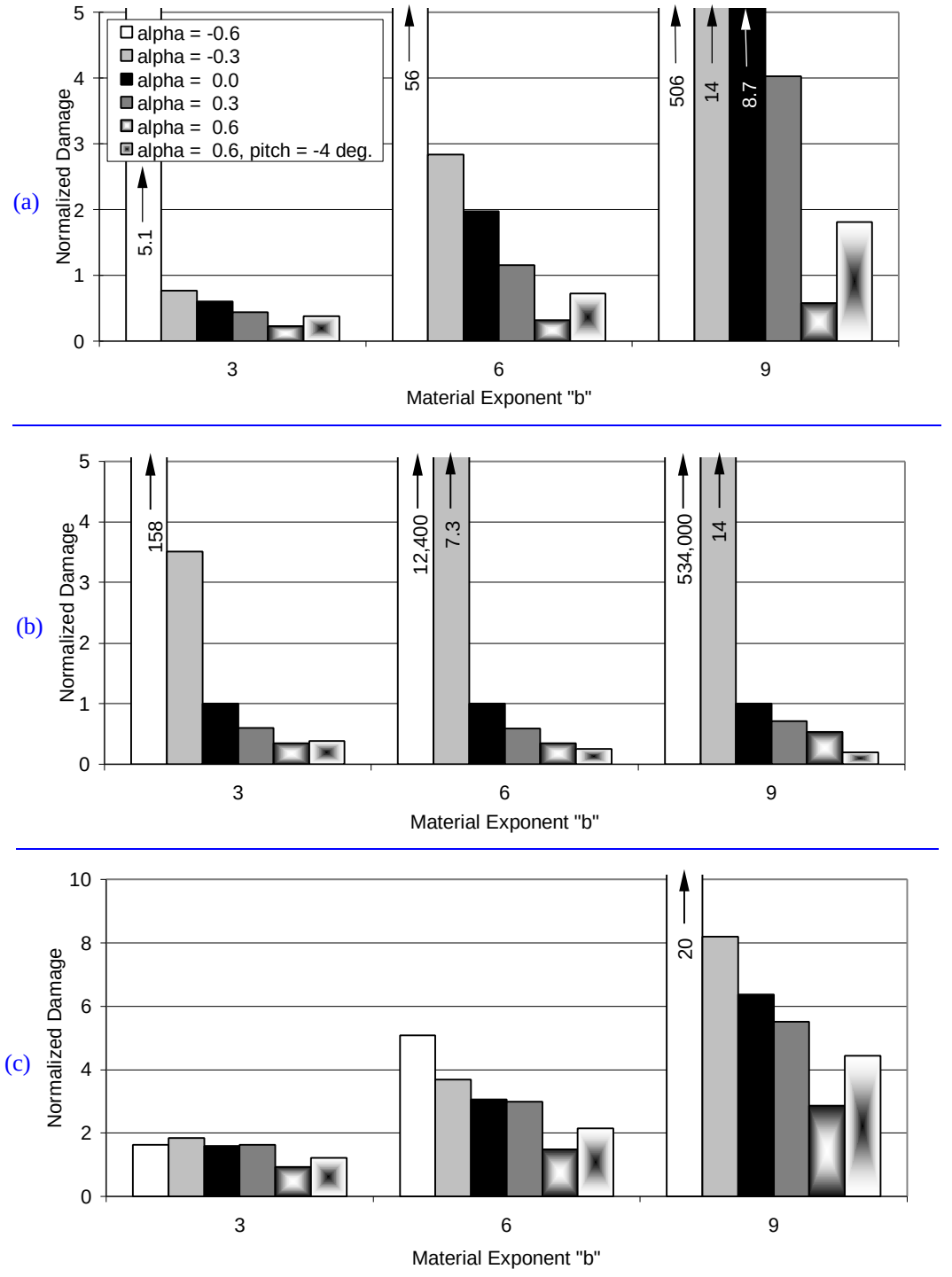

Figure 5. Comparison of relative fatigue damage for 6 blade models and 3 material exponents for 100 simulated minutes at (a) 8, (b) 14, and (c) 20 m/s average wind speed with 50% IEC turbulence intensity.

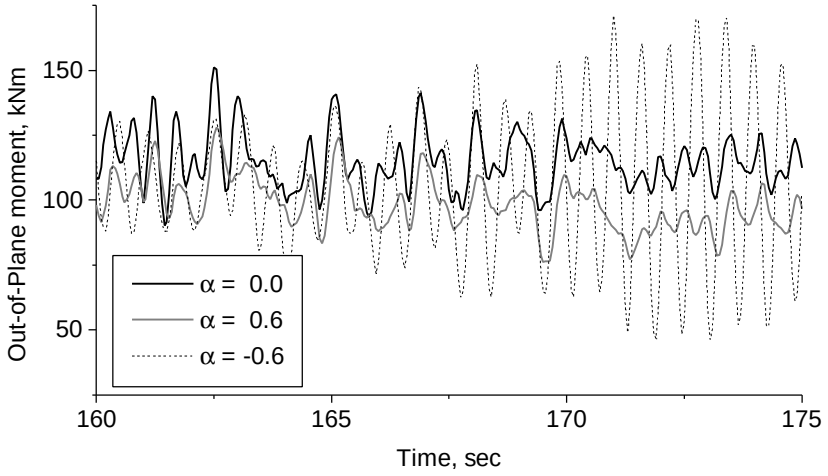

Figure 6. Time series plot of blade bending moment demonstrating the instability of the α =-0.6 model.

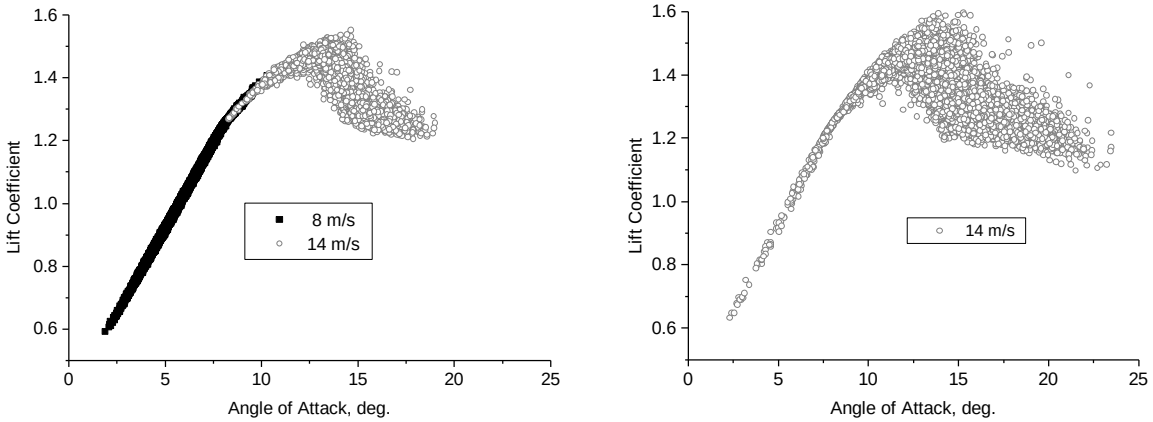

(a) (b)

Figure 7. Coefficient of lift plots showing the range for 8 m/s (solid black squares) is greater than that for 14 m/s (open gray circles) for the low turbulence case (a), and both are smaller than for the 14 m/s high turbulence case (b).

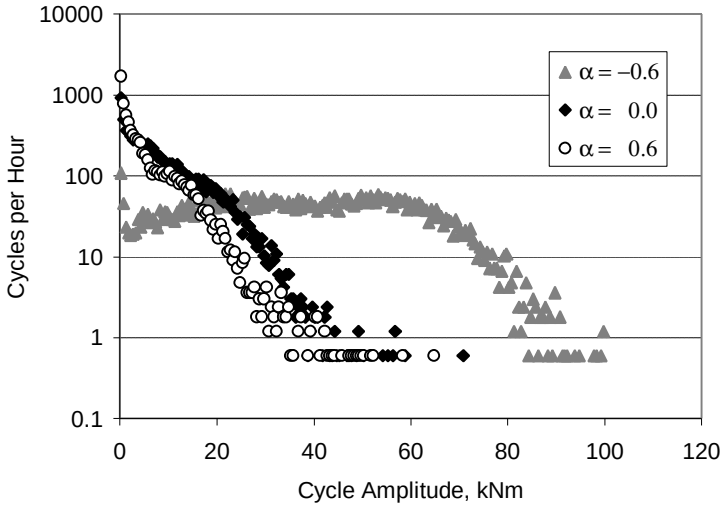

Figure 8. Comparison of cycle counted out-of-plane bending moment from 100 simulated minutes for 3 models at 14 m/s wind speed with IEC turbulence intensity.

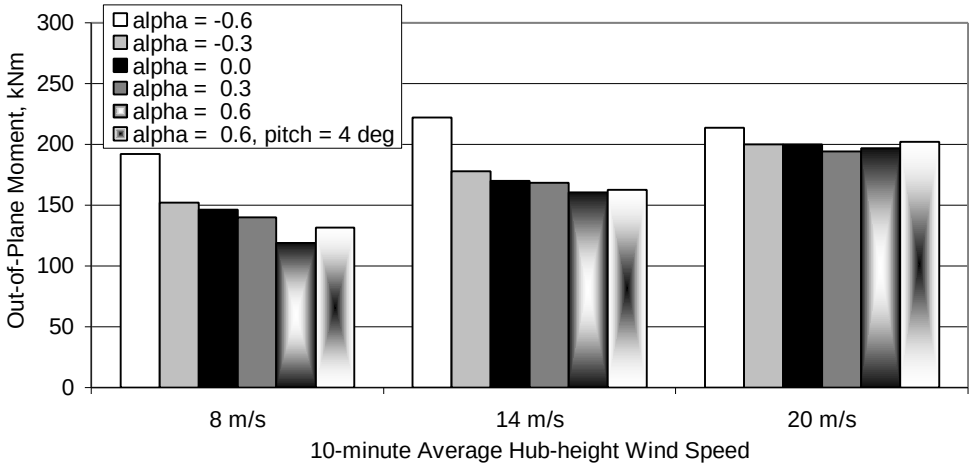

Figure 9. Comparison of maximum out-of-plane moments over all simulations for all models and wind speeds.

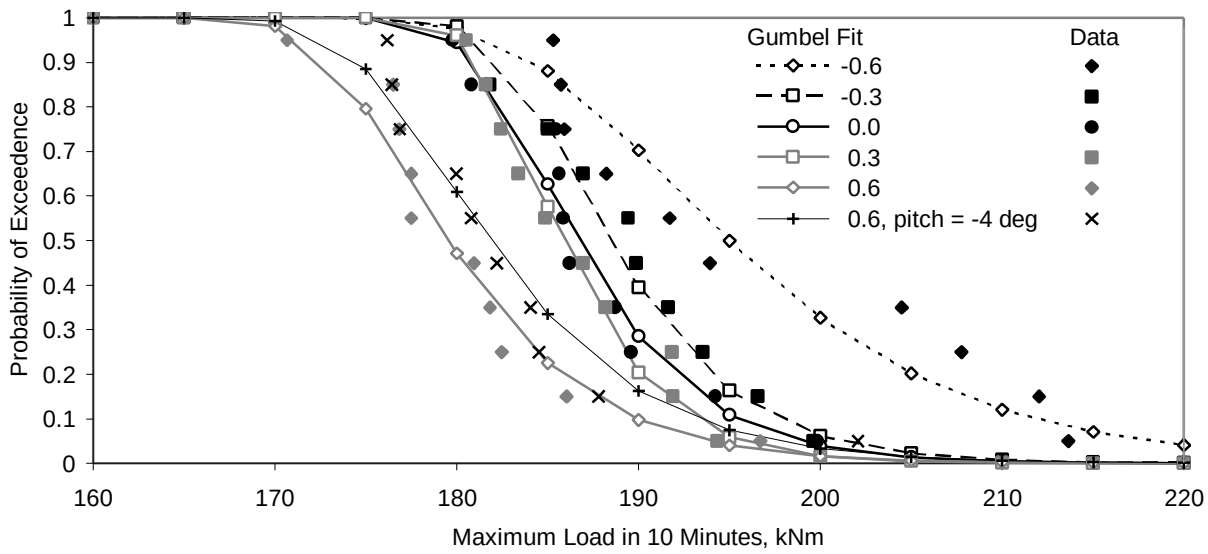

Figure 10. Comparison of curves of probability of exceedence in 10 minutes at 20 m/s average wind speed and associated simulation data points for maximum out-of-plane moment for all 6 wind turbine models.

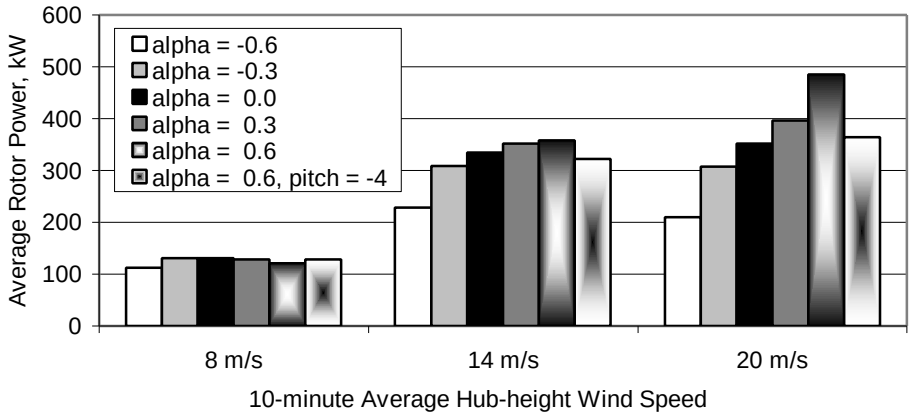

Figure 11. Comparison of average rotor power over all simulations for all models and wind speeds.